Trop J Phytochem Pharm Sci, March 2025; 4(3): 141 – 149 **ISSN 2955-1226 (Print)**
ISSN 2955-123(Electronic)

Tropical Journal of Phytochemistry & Pharmaceutical Sciences

Available online at https://www.tjpps.org

Original Research Article

Multiscale Computational Investigations of Keap1 Inhibitors for Kidney Disease Treatments: Integrating *in silico* and *in vivo* Approaches

Lucky O Iserhienrhien [1*] and Habibah Danesi [1]

[1] *Department of Biochemistry, Faculty of Basic Medical Sciences, College of Medical Science, Edo University Iyamho, Km 7 Auchi-Abuja Road, Iyamho-Uzairue, P.M.B. 04, Auchi, Nigeria.*

ABSTRACT

Kidney injury, a growing global health concern, lacks effective therapeutic interventions. This study aimed to identify natural compounds from *Geophila obvallata* (Gob) that modulate the Keap1/Nrf2 pathway, a key mediator of cadmium-induced nephrotoxicity. Eighty-five bioactive compounds from Gob were screened via molecular docking, quantitative structure-activity relationship (QSAR) modeling, and absorption, distribution, metabolism, excretion, toxicity (ADMET) profiling against Keap1. The top candidates, Quercetin-3-rhamnoside (Q3R) and Narcissin, along with the reference compound Resveratrol, were further evaluated using 100-ns molecular dynamics (MD) simulations. The Q3R-Keap1 complex demonstrated superior conformational stability (RMSD: 1–3 Å), outperforming Resveratrol. To validate these computational insights, an *in vivo* study was conducted with 28 male mice divided into four groups: control, Cd-exposed (0.3 mg/kg), Cd + Q3R (0.3 mg/kg Cd + 50 mg/kg Q3R), and Q3R alone (50 mg/kg). Treatments were administered via oral gavage for 28 days. Cadmium exposure significantly increased blood urea nitrogen (BUN) and creatinine levels, elevated reactive oxygen species (ROS: 9.93 U/mg tissue) and malondialdehyde (MDA: 5.03 nmol/mg protein), and suppressed antioxidant enzymatic activities (GPx, GSH, GST, CAT, SOD). Q3R co-administration significantly attenuated cadmium-induced renal dysfunction BUN (46.78 mg/dL vs. 72.24 mg/dL; creatinine: 1.03 vs. 2.48 mg/dL), reversed oxidative stress markers, and restored antioxidant enzyme activity. These findings demonstrate the potential of integrated computational and natural product approaches in developing novel therapies for kidney diseases.

Keywords: Kidney injury, Quercetin-3-rhamnoside, *Geophila obvallata*, Molecular dynamic simulations, Molecular docking

Received 30 January 2025
Revised 06 March 2025
Accepted 28 March 2025
Published online 01 April 2025

Introduction

Heavy metal contamination of water sources, particularly cadmium (Cd), presents a significant global public health challenge. [1] Proximal tubules of nephrons are primary targets where Cd disrupts mitochondrial electron transport chains, leading to dysfunction of renal epithelial cells via bioaccumulation. [2] Chronic cadmium exposure induces nephrotoxicity through mitochondrial dysfunction and oxidative stress, yet current therapies remain palliative, underscoring the need for mechanism-driven interventions. [3]

The Keap1/Nrf2 signaling pathway, which plays a crucial role in regulating antioxidant defenses, has become a significant focus for potential treatments in kidney injury (KI) -related disease processes. When cells experience oxidative damage, Nrf2 dissociates from Keap1, translocates to the nucleus, and activates genes that help protect cells from harm.

*Corresponding author. Email iserhienrhien.lucky@edouniversity.edu.ng

Tel: +2348066511869

Citation: Iserhienrhien LO, Danesi H. Multiscale Computational Investigations of Keap1 Inhibitors for Kidney Disease Treatments: Integrating in silico and in vivo Approaches. Trop J Phytochem Pharm Sci. 2025; 4(3) 141 – 149 http://www.doi.org/10.26538/tjpps/v4i3.6

Official Journal of Natural Product Research Group, Faculty of Pharmacy, University of Benin, Benin City, Nigeria.

However, cadmium (Cd) exposure disrupts this pathway, exacerbating oxidative damage and inflammation. [4] Restoring Keap1/Nrf2 signaling could mitigate Cd-induced nephrotoxicity; however, synthetic Nrf2 activators often suffer from off-target effects and poor bioavailability. [5] This limitation has spurred interest in natural compounds, which provide multi-target modulation with fewer side effects. [6]

Notably, *Geophila obvallata* (Rubiaceae), a traditional diuretic remedy, exhibits unexplored potential as a source of Keap1/Nrf2 modulators, addressing gaps in phytochemical research. [7] Studies have confirmed their antioxidant and renoprotective effects in toxin-induced nephropathy models; [8-10] however, its bioactive compounds and mechanisms of action against Cd toxicity remain largely unexplored. Modern drug discovery increasingly utilizes computational tools such as molecular docking, ADMET profiling, and molecular dynamics (MD) simulations to expedite the identification of natural drug candidates. [11] For instance, molecular docking and Molecular Mechanics/Generalized Born Surface Area (MM/GBSA) analyses have successfully predicted plant-derived inhibitors of Keap1/Nrf2 pathway in previous studies. [12, 13] These methods reduce experimental costs by prioritizing high-affinity ligands for *in vivo* validation, making them indispensable for phytochemical research. While previous studies have highlighted Gob's antioxidant potential, [13] no research has investigated its phytochemicals as Keap1/Nrf2 modulators in Cd-induced KI. This study aims to address these gaps by integrating computational screening (AutoQSAR, ADMET, MD simulations) with *in vivo* validation to identify Gob-derived Keap1/Nrf2 inhibitors. Additionally, it leverages machine learning (AutoQSAR) to predict toxicity and optimize lead compounds—a strategy that has rarely been applied to nephroprotective

phytochemicals. This study seeks to identify and validate *Geophila obvallata*-derived phytochemicals as potential therapeutic agents to mitigate the nephrotoxic effects of cadmium exposure.

Materials and Methods

Structure Preparation for Molecular Docking

The Keap1 kelch domain structure (PDB ID: 6ZEY), which includes a bound inhibitor (5-cyclopropyl-1-[3-(phenylsulfonylamino) phenyl] pyrazole-4-carboxylic acid), was downloaded from the Protein Data Bank. To optimize the protein for docking studies, Schrödinger's computational tools [14] were used to refine the structure. This involved multiple steps: deleting nonessential water molecules, adding hydrogen atoms, adjusting protonation states to reflect neutral pH conditions (7.0 ± 2.0) via PROPKA, and refining the geometry through energy minimization with the OPLS3e parameters. [14]

Ligand preparation

Eighty-five phytochemicals from *Geophila obvallata* (Gob), previously characterized via GC-MS [9] and HPLC, [16] were selected for analysis. Molecular structures were obtained from the PubChem repository and processed with Maestro's module to refine their 3D conformations and physicochemical properties. Subsequent preparation and optimization of the structures were performed using Maestro's LigPrep tool.

Glide Grid Generation

Receptor grid files were generated using Schrödinger's Glide module within the Maestro workspace. The grid coordinates (x, y, z) for the Keap1 crystal structure (PDB ID: 6ZEY) were defined as 3.55, −44.92, and −7.19, respectively. These grids identified favorable ligand-binding regions to guide subsequent docking simulations.

In Silico Exploration of Structure-Activity Relationships (QSAR)

A QSAR model was trained on a dataset of experimentally validated Keap1 inhibitors (ChEMBL database) with corresponding pIC50 values using Schrödinger's AutoQSAR tool. [11] The model generated descriptors, selected features, and identified the optimal algorithm. Performance metrics included training set R^2 (75%) and test set Q^2 (25%). The top model predicted pIC50 values for lead compounds to prioritize biological activity.

Virtual Screening

A dual-filter virtual screening workflow was applied to 85 ligands. Lipinski's Rule of Five [16] eliminated 45 compounds, retaining 40 for further analysis. Subsequent screening combined QSAR predictions (kpls_linear_13 model) and MM/GBSA calculations, selecting 20 compounds with pIC50 > 6.0 nM as leads.

Docking and MM/GBSA Calculations

The seven most promising candidates identified through screening were subjected to high-precision (XP) molecular docking. To evaluate interaction strength, binding free energy values were estimated using Schrödinger's Prime MM/GBSA computational method. This involved calculating energy differences between optimized protein-ligand configurations and their isolated counterparts to determine complex stability. [14, 15]

Toxicological Characterization

ADMET properties of five leads and a standard drug were predicted using the AdmetSAR v3 web server (http://lmmd.ecust.edu.cn/) to evaluate pharmacokinetics and safety.

MD simulation

Molecular dynamics (MD) simulations (100 ns, NPT ensemble) were performed using Desmond (Schrödinger) for the top two ligands and Resveratrol. The system was prepared with the TIP3P solvent model in a 10 × 10 × 10 Å³ orthorhombic box, neutralized with Na^+/Cl^- ions, and minimized with the OPLS4 force field. Stability was assessed via RMSD and RMSF analyses. [14]

Research Facilities

Biochemical analyses: Biochemistry Laboratory, Federal University of Technology, Akure, Nigeria. Bioinformatics and Gene expression: Teady Bioscience Laboratory, Akure, Nigeria.

Reagents and Chemicals (Grade, Purity, Manufacturer)

Cadmium chloride ($CdCl_2$): 99.9% purity, CAS No. 10108-64-2, Sigma-Aldrich (St. Louis, MO, Germany). Quercetin-3-rhamnoside (Q3R): ≥98% HPLC purity, PhytoLab GmbH and Co. KG (Vestenbergsgreuth, Germany). Isoflurane: 100% pharmaceutical grade, Piramal Critical Care (Bethlehem, PA, USA). RNAlater Stabilization Solution: Thermo Fisher Scientific (Waltham, MA, USA). RNeasy Maxi Kit: Qiagen (Hilden, Germany). SYBR Green PCR Master Mix: Applied Biosystems (Foster City, CA, USA). TaqMan Reverse Transcription Reagents: Thermo Fisher Scientific (Waltham, MA, USA). Randox BUN and creatinine assay kits: Randox Laboratories (Crumlin, UK). All other chemicals: Analytical grade (≥95% purity), Merck KGaA (Darmstadt, Germany).

Equipment and Instruments (Model, Manufacturer)

Spectrophotometer: Shimadzu UV-1800 UV-Vis Spectrophotometer. Thermal cycler: Bio-Rad T100 Thermal Cycler (CA, USA). Centrifuge 5424 R: Eppendorf (Hamburg, Germany). Autoclave (SX-500): Tomy Digital Biology (Tokyo, Japan). cDNA synthesizer: Applied Biosystems High-Capacity cDNA Reverse Transcription Kit (Cat. No. 4368814) (San Jose, CA, USA). Freezer (-80°C): Thermo Fisher Scientific Revco ULT Freezer.

Animal model and ethical compliance

Twenty-eight male Wistar albino mice (38–40 g) were housed under controlled conditions (22 ± 2°C, 50–60% humidity, 12-hour light/dark cycle) and fed *ad libitum*. Ethical approval (IBR/EUIEC/2023/028) was obtained from Edo University, adhering to EU Directive 2010/63/EU. [17]

Experimental design

Mice were randomly divided into four groups (n = 7/group) using stratified randomization (GraphPad Prism 10.0.2): Control: Received 0.9% saline (vehicle). $CdCl_2$ group: 6.5 mg/kg/day $CdCl_2$ (oral gavage). [17] $CdCl_2$ + Q3R group: 6.5 mg/kg/day $CdCl_2$ + 50 mg/kg/day Q3R. [18] Q3R group: 50 mg/kg/day Q3R. Dosing rationale: $CdCl_2$ dose selected based on Asagba and Obi (2004), [17]; Q3R dose optimized from prior subacute toxicity studies. [9] Treatments were administered daily for 28 days using a 22-gauge oral gavage needle (Instech Laboratories, USA). On day 28, mice were euthanized via 5% isoflurane inhalation. Blood was collected via cardiac puncture, and kidneys were perfused with cold 1.15% KCl.

Biochemical and molecular assays

Catalase (CAT) activity was measured via hydrogen peroxide decomposition at 240 nm. [19] Superoxide dismutase (SOD) activity was assayed using nitroblue tetrazolium reduction inhibition at 560 nm. [20] Glutathione peroxidase (GPx), GST, and GSH were quantified using Ellman's reagent (412 nm). [21] The antioxidant activities of catalase (CAT) and superoxide dismutase (SOD) were assessed using the method described by. [20] The activities of glutathione peroxidase (GPx), glutathione S-transferase (GST), and reduced glutathione (GSH) were evaluated according to the procedures outlined by. [21]

Assessment of Oxidative Stress Biomarkers

The levels of reactive oxygen species (ROS) were determined using the dichlorofluorescein fluorescence method described by. [22] Malondialdehyde (MDA) levels, a marker of lipid peroxidation, was

measured using thiobarbituric acid reactive substances (TBARS) at 532 nm. [23]

Evaluation of Renal Function Parameters

Blood urea nitrogen (BUN) and serum creatinine concentrations, indicators of renal function, were measured using the method described by [24] with Randox kits (Cat. No. UR2125 and CR5101) per manufacturer protocols.

Gene Expression Analysis

The expression profiles of Keap1, Nrf2, KIM-1, and HO-1 were quantitatively assessed via qRT-PCR, with GAPDH serving as the internal reference gene. The Fast Quant RT kit was employed, following the protocol outlined by. [25] Total RNA was extracted from kidney tissues using RNeasy Maxi kits. RNA integrity (RIN > 8.0) was confirmed via Agilent 2100 Bioanalyzer; β-actin served as the housekeeping gene. cDNA was synthesized with TaqMan Reverse Transcription Reagents (1 µg RNA, random hexamers). qRT-PCR Amplification was performed on an ABI Prism 7900HT system using SYBR Green Master Mix. The primer sequences are captured in Table 1 below:

Table 1: Sequences and primers for molecular studies

S/N	Genes	Sequence for forward primer	Sequence for reverse primer	GenBank accession number
1	*Keap1*	GAG GTT AGG AGT TTA AGG	CAA CCA AAC CCC CCT TCT C	NC_000019.10
2	*Nrf2*	TTCACTAAAC ACAAGTCCCA GT	CAGGGGCACTA TCTAGCTCT	NM_031782
3	*Kim-1*	TGGCACTGTG ACATCCTCAG A	GCAACGGACAT GCCAACATA	NM_173149
4	*Ho-1*	CACAGCCACT TTCCACACAG	TTTGCTCCACA GATTTCAGA	NC_086037.1
5	β - actin	AGACAGCCGC ATCTTCTTGT	CTTGCCGTGGG TAGAGTCAT	NM_031144

Data analysis

Data are expressed as mean ± SEM. Statistical significance ($p < 0.005$) was determined using one-way ANOVA with Tukey's HSD post-hoc test (GraphPad Prism 10.0.2, San Diego, CA, USA, 2023). Raw data and statistical outputs are provided in Supplementary File Table S2 and Table S3.

Results and Discussion

Table S1 summarizes the initial screening of 85 compounds derived from *Geophila obvallata* (Gob) for potential Keap1 inhibitors. Lipinski's Rule of Five (Ro5) [16] serves as a foundational guideline for predicting essential pharmacokinetic characteristics, such as oral absorption and membrane permeability. Molecules that exceed its thresholds—including molecular weights greater than 500 Daltons, logP values above 5, more than five hydrogen bond donors, or over 10 nitrogen or oxygen atoms—tend to exhibit reduced absorption and bioavailability. [14] By applying Ro5, researchers can prioritize compounds with favorable drug-like properties, thereby avoiding those with limited therapeutic potential, which is a crucial step in early drug discovery. [25]

The Ro5-based screening excluded 44 compounds with suboptimal pharmacokinetic profiles, reducing the library to 41 candidates (Table S1; Table 2). These results are consistent with the findings of Genheden and Ryde (2015), [26] who emphasized the utility of Ro5 in virtual screening.

To prioritize inhibitors, a QSAR analysis was conducted to correlate molecular structure with predicted bioactivity (Figure 1). The kpls_radial_46 model ($R^2 = 0.8298$, $Q^2 = 0.8244$, RMSE = 0.5198) predicted pIC50 values, excluding compounds with values less than 6.00 nM (Table 2). This machine learning model demonstrated strong predictive accuracy, refining the library to include compounds with high bioavailability and target affinity (Table 3). These steps align with established workflows, such as those described by Alzain *et al.* (2023), [27] who employed *in silico* methods to identify natural Nrf2/Keap1 modulators for cancer therapy.

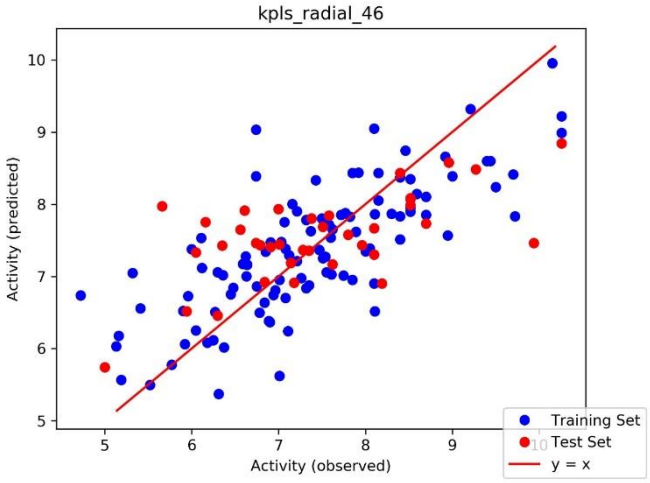

Figure 1: Data visualization (scatter plots) and optimal parameters of the AutoQSAR model for predicting activity in Keap1.

Table 2: Bioactivity of the lead compounds against 6ZEY as predicted by QSAR Models

6ZEY

Lead compounds	**pIC$_{50}$**
Narcissin	6.090
Rutin	6.419
Quercetin-3-rhamnoside	6.090
Birutan	6.120
Hyperin	6.120
Resveratrol (Standard)	6.120

Table 3: In silico-predicted pharmacological profiles of the lead compounds targeting the 6ZEY receptor.

6ZEY					
Model Code	Score	S.D	R^2	RMSE	Q^2
Kpls_radial_46	0.8258	0.5508	0.8298	0.5198	0.8244

Figures 2 and 3 illustrate the Extra Precision (XP) docking of the top 10 compounds compliant with the RO5. XP docking is regarded as a more rigorous and accurate method compared to Standard Precision (SP) docking. [28] The analysis identified nine high-affinity Keap1 binders with docking scores ranging from -6.610 kcal/mol (Resveratrol) to -12.49 kcal/mol (Table 4). Resveratrol, the reference compound, exhibited limited interactions forming three hydrogen bonds with ILE416, ALA366, and LEU365 as well as a pi-interaction with ARG483. In contrast, leading candidates like Quercetin-3-rhamnoside (Q3R) and Coniferyl ether established extensive interaction networks: Q3R formed seven hydrogen bonds (with TYR334, SER363, ASN414,

SER555, ARG380, SER602), while Coniferyl ether formed eight (with ARG483, ARG415, ASN414, SER363, GLY433, SER431, ASP389, and ASN382, GLY364). These interactions indicate superior binding specificity compared to Resveratrol. These findings align with the research conducted by Hagar *et al.* (2020) [29] who investigated various antiviral N-heterocycles using similar biocompounds.

MMGBSA calculations further corroborated these findings, with binding energies for the top compounds ranging from -24.22 to -13.59 kcal/mol, surpassing that of Resveratrol at -13.59 kcal/mol (Table 4). These calculations provide an estimate of the free energy of binding and can help refine the ranking of target ligands. [30] Similar studies by Liu *et al.* (2023) [31] have demonstrated that enhanced affinity likely arises from the ligands' ability to interact with critical protein residues, such as ARG483 and SER555 in Keap1, which are involved in Nrf2 binding. This interaction competitively inhibits Keap1-Nrf2 interactions.

Table 5 presents the ADMET test results for the top-scoring compounds. A significant limitation observed in most of the screened compounds screened was their low gastrointestinal (GI) absorption, low Caco-2 permeability, inhibition of OATP and CYP enzymes, as well as prediction of organ, mitochondrial, and hemolytic toxicity. These findings raise concerns about their safety profiles, which effectively disqualifies them from consideration for patient compliance. [32-33] However, among the evaluated compounds, Quercetin-3-rhamnoside (Q3R) stands out due to its more favorable ADMET profile, positioning it as a promising lead candidate. Its high GI absorption, combined with negligible mitochondrial and hemolytic toxicity, suggests potential for improved oral bioavailability and reduced biliary excretion, respectively. BSEP inhibition can lead to increased enterohepatic recirculation of drugs, potentially enhancing their efficacy and prolonging their duration of action. [34] In contrast, Resveratrol presents risks of drug-induced liver injury (DILI) and genotoxicity (Ames test positive), highlighting Q3R's superior safety profile. This finding aligns with the report by Chi *et al*., (2024) [35] which emphasizes that ADMET scoring functions are critical for determining the chemical drug-likeness of small molecules within the body and ultimately influencing their therapeutic potential. However, this conclusion contrasts with some reports suggesting that ADMET predictions may not always accurately reflect the actual in vivo behavior of compounds. [36]

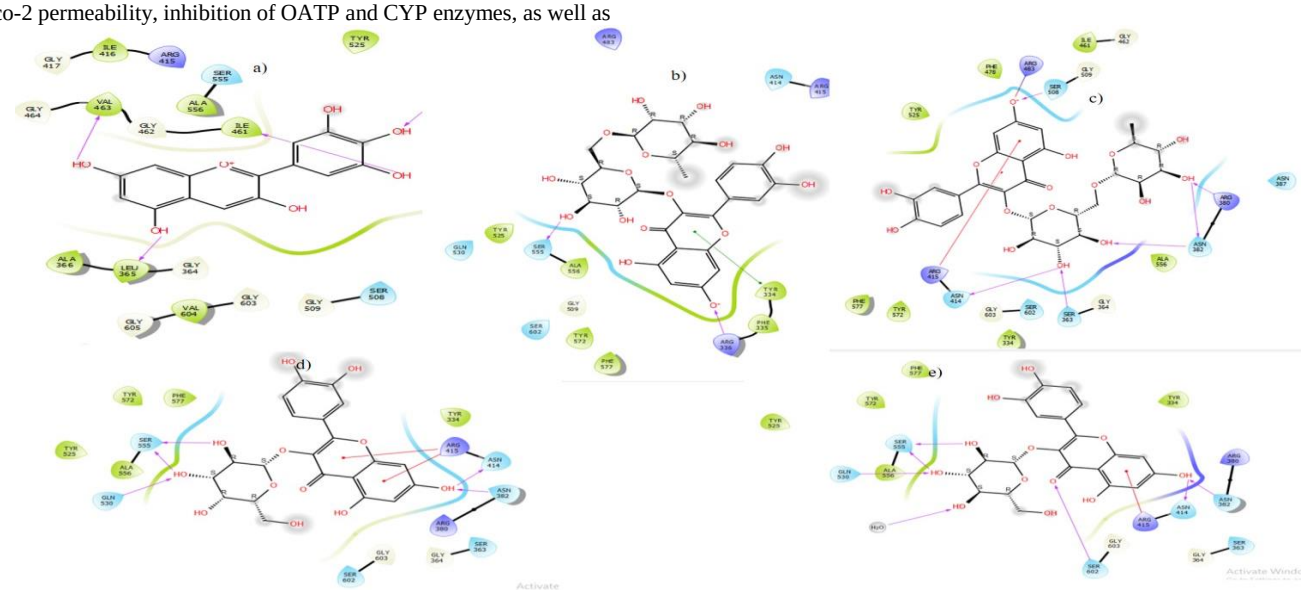

Figure 2: 2D interacting plots between a) Narcissin b) Rutin c) Birutan d) Hyperin and e) Isoquercetin with residues at the binding pocket of **Keap1**

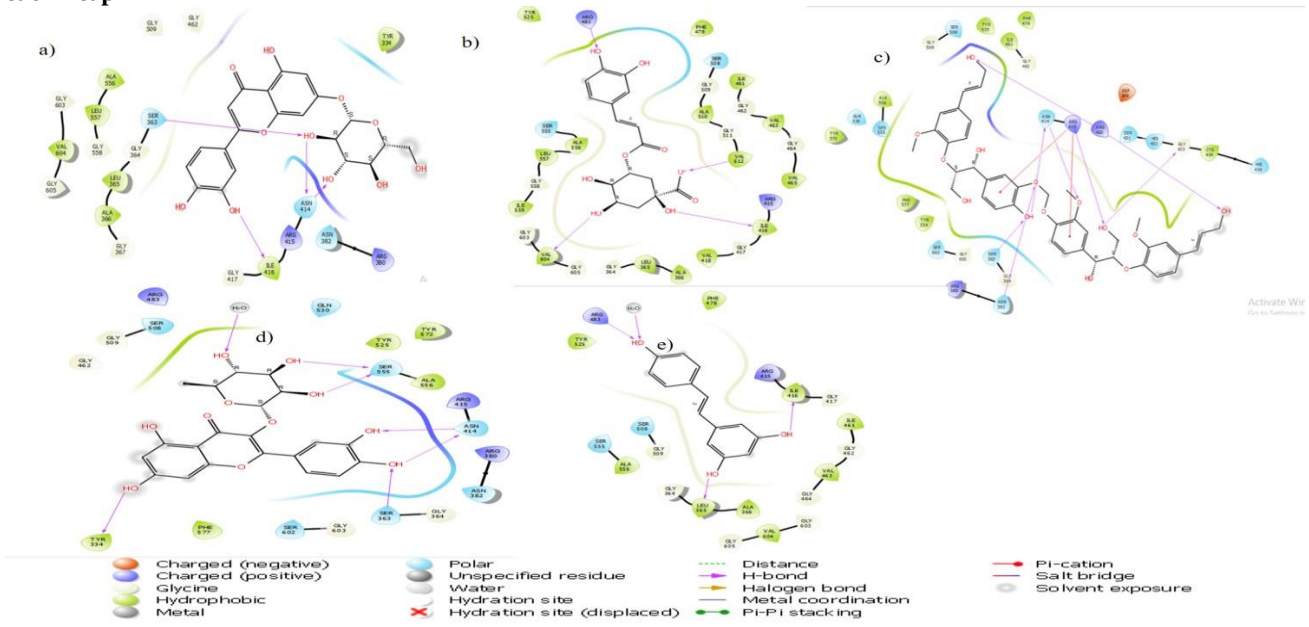

Figure 3: 2D interacting plots between a) Cyranoside b) Chlorogenic acid c) Coniferyl ether d) Quercetin 3-rhamnoside and e) Resveratrol with residues at the binding pocket of Keap1

Table 4: Molecular docking analysis results and interaction fingerprints of top-scoring ligands against KEAP 1 (6ZEY)

Bioactive compounds	XP Docking score	MMGBSA ΔG_Bind (kcal/mol)	Interacting residues/no of H-bond
Narcissin	-12.49	-19.43	VAL463, ILE461, LEU365, ARG483, PHE478, TYR525 [6 H-BONDS]
Rutin	-12.39	-22.34	ARG483, SER506 ARG380, ASN382, ALA556, SER363, ASN414, ARG415 [8 H-BONDS]
Birutan	-12.04	-22.34	TYR334, ARG336, SER555 PHE335, TYR525 [4 H-BONDS]
Hyperin	-10.66	-24.22	SER555, GLN530, ARG415, ASN414, ASN382, ARG380 [5 H-BONDS]
Isoquercetin	-10.42	-22.92	ASN382, ASN414, ARG415, SER602, GLN530 [5 H-BONDS]
Cyranoside	-9.91	-20.02	ASN414, ILE416, SER363, ARG415, ARG380 TYR334 [4 H-BONDS]
Chlorogenic acid	-9.91	-16.93	ILE416, VAL512, ARG483, VAL 604 [4 H-BONDS]
Coniferyl ether	-9.89	6123	ARG483, ARG415, ASN414, SER363, GLY433, SER431, ASP389, ASN382, GLY364 [9 H-BONDS]
Quercetin-3-rhamnoside	-9.55	-17.59	TYR334, SER363, ASN414, SER555, ARG380, SER602 [7 H-BONDS]
Resveratrol (standard)	-6.610	-13.59	ARG483, ILE416, ALA366, LEU365 [4 H-BONDS]

Table 5: ADMET profiles of selected and reference compounds

	Narcissin	**Rutin**	**Birutan**	**Hyperin**	**Isoquercetin**	**Cynaroside**	**Chlorogenic acid**	**Coniferyl ether**	**Quercetin-3-rhamnoside**	**Resveratrol (standard)**
Absorption										
GI Absorption	Low	Low	Low	Low	Low	Low	Low	High	High	High
HIA	Low	Low	Low	Low	Low	High	Low	Low	High	High
CaCO-2 Permeability	Low	Low	Low	Low	Low	Low	Low	Low	Low	High
Distribution										
BBB	No	No	No	No	No	No	No	No	No	Yes
OATP1B1 inhibitor	Yes	Yes	Yes	Yes	Yes	Yes	Yes	Yes	Yes	Yes
BSEP inhibitor	No	No	No	No	No	No	No	No	Yes	Yes
Metabolism										
CYP1A2 inhibitor	No	No	No	No	No	No	No	Yes	No	Yes
CYP3A4 inhibitor	No	No	No	No	No	No	No	Yes	No	Yes
CYP2C9 inhibitor	No	No	No	No	No	No	No	Yes	No	Yes
CYP2C19 inhibitor	No	No	No	No	No	No	No	Yes	No	Yes
CYP2D6 inhibitor	No	No	No	No	No	No	No	Yes	No	No
Excretion										
CLp	No	No	No	Yes	Yes	Yes	No	No	Yes	Yes
CLr	Yes	Yes	Yes	Yes	Yes	Yes	Yes	Yes	Yes	Yes
Toxicity (Mouse)										
Ames Test	No	No	No	No	No	No	No	No	Yes	Yes
Mitochondrial toxicity	Yes	Yes	No	Yes	Yes	Yes	No	No	Yes	Yes
Hemolytic toxicity	Yes	Yes	Yes	No	No	Yes	Yes	Yes	No	No
Nephrotoxicity	No	No	No	No	No	No	No	No	No	No
DILI	No	No	No	No	No	No	No	No	No	Yes
hERG	No	No	No	No	No	No	No	No	No	No

Abbreviations: Human intestinal absorption (HIA), Characterization of colorectal adenocarcinoma cell line (Caco-2), Blood brain barrier (BBB), Organic anion transporting polypeptide (OATP1B1), Bile salt export pump (BSEP), Plasma clearance (CLp), Renal clearance (CLr), Human ether-a-go-go-related gene (hERG), Drug induced liver injury (DILI)

ISSN 2955-1226 (Print)
ISSN 2955-123(Electronic)

Figures 4-6 illustrate the Molecular Dynamics (MD) simulations of three ligand-protein complexes. This study utilized MD simulations to investigate the binding interactions and conformational stability of three Keap1 complexes (Figure 4): (a) Q3R-Keap1, (b) Narcissin-Keap1, and (c) Resveratrol-Keap1. The root mean square deviation (RMSD) values for both the protein alpha carbons (Cα) and ligand's fit to the protein were plotted. The Q3R-Keap1 complex demonstrated excellent stability throughout the simulation, with low root mean square fluctuation (RMSF) values (0–2.0 Å) (Figure 5a) and only minor fluctuations observed at the very beginning (0-9 ns). The RMSD remained within a narrow range (1-3 Å), indicating that Q3R maintained a stable binding pose within the Keap1 pocket. In contrast, the Narcissin and Resveratrol complexes exhibited significant fluctuations (RMSD peaks at 20–64 ns and 78 ns, respectively) and elevated RMSF values (2.4–2.8 Å) in residues 50–60, a region critical for Keap1-Nrf2 binding (Figures 5b-c). [37]

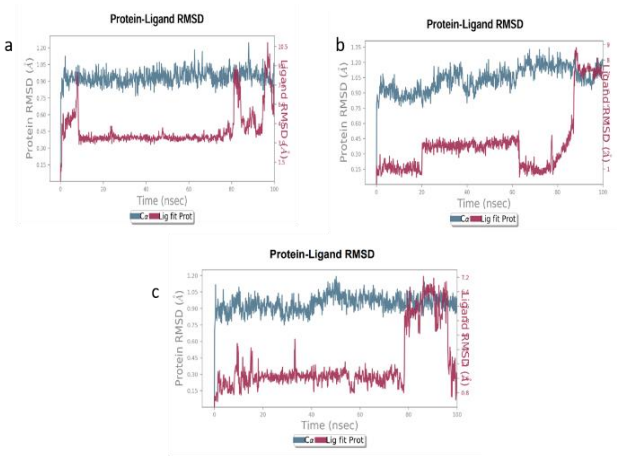

Figure 4. RMSD profiles for Cα atoms of Keap1 (blue) and Ligand-Prot complexes (red) were plotted over a 100 ns simulation timeframe for (a) Q3R, (b) Narcissin, and (c) Resveratrol (standard), providing insights into structural stability.

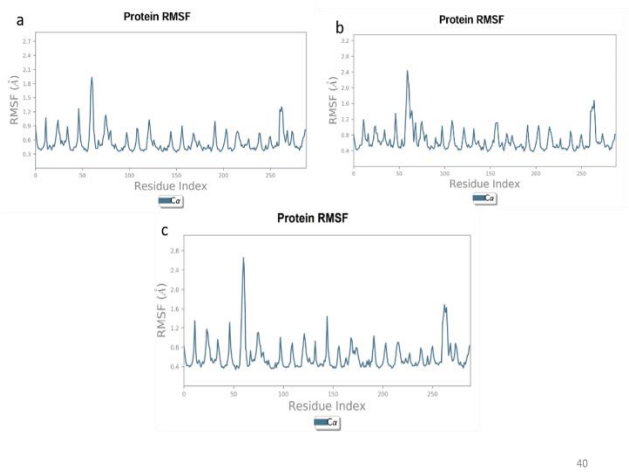

Figure 5. Dynamic fluctuations of Keap1's Cα atoms are visualized through line representations, illustrating the temporal evolution of RMSF during simulations with (a) Q3R, (b) Narcissin, and (c) Resveratrol (standard).

This suggests a strong and specific interaction between Q3R and Keap1, demonstrating potent inhibitory effects on Keap1-Nrf2 signaling. These findings align with earlier research [38] that employed computational screening strategies focused on structure and substructure exploration of existing compounds to identify inhibitors of the Keap1-Nrf2 interface. By analyzing MD trends, the study gained comprehensive insights into the stability, movement patterns, and interaction geometries of the complexes during the simulation. This analysis not only reinforced the accuracy of docking predictions but also highlighted key areas for guiding further refinement of the molecules. [14]Figure 6 illustrates the distinct interaction patterns of protein-ligand contacts for each ligand. The binding mode of Q3R reveals a multifaceted network of interactions, including hydrogen bonds, non-polar contacts, and electrostatic interactions with key residues lining the Keap1 binding pocket. This diverse interaction network likely contributes to the high stability and strong binding affinity observed for Q3R. [38] These findings align with the report by Kolacz *et al.* (2017), [39] which suggests that while target ligands may interact with Keap1, their binding modes can differ significantly from those of hit compounds, potentially affecting their inhibitory activity. These discoveries have significant implications for elucidating the intricate molecular mechanisms governing the interplay between these compounds and Keap1, as well as their potential utility as therapeutic interventions for diseases characterized by aberrant Keap1-Nrf2 signaling pathways. [40] However, it is important to note that the 100-ns simulation time may not have been sufficient to fully explore potential conformational changes or dissociation events, particularly for less stable complexes such as Narcissin-Keap1 and Resveratrol-Keap1.

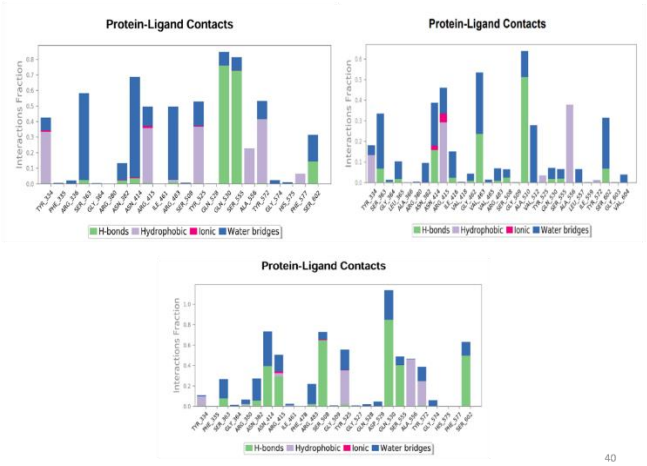

Figure 6. (Color online) Spatial mapping of protein-ligand interactions reveals key binding modes for (a) Q3R, (b) Narcissin, and (c) Resveratrol (standard).

Table 6 summarizes the effects of cadmium (Cd) exposure and Q3R treatment on key biochemical parameters in mice. The concentration of malondialdehyde (MDA), an indicator of lipid peroxidation increased by 2.3-fold, while the activities of antioxidant enzymes such as GPx, GSH, GST, CAT, and SOD by 40–60% due to significant Cd exposure. The findings of this experiment corroborate earlier research that highlights cadmium's role in triggering oxidative damage and inflammatory processes within renal tissues. [41] Q3R significantly attenuated the Cd-induced increase in MDA levels and restored the activities of GPx, GSH, GST, CAT, and SOD to control levels ($p < 0.05$). These results demonstrate that Q3R possesses potent antioxidant properties and effectively mitigates the oxidative damage caused by Cd exposure. The nephroprotective properties of Q3R revealed in this investigation align closely with our *in silico* findings.

Table 7 presents the renal function parameters in mice treated with cadmium (Cd), Q3R, or a combination of both. Blood urea nitrogen (BUN) levels were significantly elevated in the Cd-only group compared to the control group ($p < 0.05$). Serum creatinine concentrations exhibited a marked increase in animals exposed solely to cadmium relative to untreated controls ($p < 0.05$). Notably, the administration of Q3R alongside cadmium mitigated the cadmium-induced increases in both BUN and creatinine levels ($p < 0.05$). Animals receiving Q3R alone showed no significant changes in these renal markers compared to untreated controls. These results are consistent with previous research indicating that cadmium exposure leads to both short- and long-term renal damage, marked by tubular cell death, glomerular impairment, and fibrous tissue accumulation in kidney structures. [42] Importantly, our findings demonstrate that co-treatment with Q3R significantly reduces the cadmium-induced elevation in both BUN and serum creatinine levels. This finding strongly suggests that Q3R plays a protective role in renal function during kidney injury. The kidney-protective effects of Q3R likely stem from its ability to activate the Nrf2-ARE signaling pathway. This pathway activation stimulates the expression of a network of genes involved in cellular defense mechanisms, including enzymes that neutralize free radicals, proteins that facilitate toxin elimination (phase II metabolism), and molecules that suppress inflammatory responses. [43] By inhibiting Keap1, Q3R can effectively activate Nrf2, thereby mitigating the harmful effects of cadmium on renal function. [44]

Table 6: Effect of Cd and Q3R on biochemical parameters

Groups	MDA (nmol/mg protein)	ROS (Umg^{-1} tissue)	GPx (unit/mg of wet tissue)	GSH (µmol/g tissue)	GST (unit/mg of wet tissue)	CAT (unit/mg of wet tissue)	SOD (unit/mg of wet tissue)
Control	0.29 ± 0.06^{a}	1.32 ± 0.13^{a}	14.20 ± 0.14^{a}	16.14 ± 0.09^{a}	13.78 ± 0.23^{a}	2.58 ± 0.02^{a}	9.46 ± 0.28^{a}
Cd only	5.03 ± 0.12^{c}	9.93 ± 0.71^{c}	7.92 ± 1.00^{c}	6.48 ± 0.01^{c}	9.88 ± 0.31^{c}	0.46 ± 0.01^{c}	2.60 ± 0.13^{c}
Cd + Q3R	4.80 ± 0.19^{b}	2.94 ± 0.11^{ab}	11.56 ± 0.16^{ab}	10.98 ± 0.20^{b}	10.98 ± 0.15^{bc}	1.88 ± 0.10^{b}	6.82 ± 0.01^{b}
Q3R only	2.65 ± 0.01^{ab}	2.28 ± 0.13^{ab}	13.20 ± 0.20^{a}	10.12 ± 0.06^{b}	11.82 ± 0.13^{ab}	2.28 ± 0.13^{a}	7.08 ± 0.14^{ab}

Data were expressed as mean ± standard error of the mean (SEM). Group comparisons were analyzed with Tukey's post hoc test, where significance thresholds were defined as (a) $P < 0.005$ versus untreated controls and (b) $P < 0.05$ relative to cadmium-exposed animals.

Table 7: Renal function impacts of Cd and quercetin-3-rhamnoside treatment.

Groups	BUN (mg/dL)	Serum creatinine (mg/dL)
Control	25.88 ± 1.24^{a}	0.26 ± 0.14^{a}
Cd only	72.24 ± 0.14^{c}	2.48 ± 0.01^{c}
Cd + Q3R	46.78 ± 0.18^{b}	1.03 ± 0.04^{b}
Q3R only	26.47 ± 0.00^{a}	0.40 ± 1.00^{a}

Data were expressed as mean ± standard error of the mean (SEM). Group comparisons were analyzed with Tukey's post hoc test, where significance thresholds were defined as (a) $P < 0.005$ versus untreated controls and (b) $P < 0.05$ relative to cadmium-exposed animals.

Figure 7 illustrates the modulatory effects of cadmium (Cd) and quercetin-3-rhamnoside (Q3R) on the transcriptional regulation of Nrf2, Keap1, HO-1, and KIM-1, which are key genes implicated in oxidative stress and renal injury. Nrf2 functions as a master transcriptional regulator that orchestrates the activation of cellular defense mechanisms against oxidative damage. Keap1 serves as a negative regulator of Nrf2, while HO-1 and KIM-1 are downstream targets of Nrf2 that play crucial roles in protecting against kidney injury (Figure 7a). [44] Notably, Cd exposure significantly downregulated Nrf2 mRNA expression ($p < 0.05$), whereas the co-administration of Cd and Q3R enhanced Nrf2 mRNA levels beyond those observed with Cd treatment alone ($p < 0.05$). Cadmium exposure triggered a marked upregulation of Keap1 mRNA expression ($p < 0.05$) compared to controls (Figure 7b). In contrast, Q3R treatment alone did not significantly affect Keap1 expression. However, the co-administration of Cd and Q3R mitigated the Cd-induced increase in Keap1 mRNA expression ($p < 0.05$). Furthermore, Cd exposure resulted in a significant downregulation of HO-1 mRNA expression ($p < 0.05$) relative to controls (Figure 7c). While Q3R treatment alone had a modest influence on HO-1 expression, its co-administration with Cd significantly enhanced HO-1 mRNA levels ($p < 0.05$) beyond those seen with Cd treatment alone. Conversely, Cd exposure led to a substantial upregulation of KIM-1 mRNA expression ($p < 0.05$), which was significantly reduced by co-treatment with Q3R. These results confirm that Cd exposure provokes oxidative stress and kidney injury, as evidenced by the dysregulation of Nrf2, Keap1, HO-1, and KIM-1 expression. Q3R treatment appears to counteract these effects by modulating gene expression, thereby contributing to its renoprotective properties against Cd-induced injury. [45] These findings align with previous studies demonstrating that cadmium exposure induces oxidative stress and inflammation in the kidney. [41-46] These results unequivocally demonstrate that the renoprotective properties of Q3R are, in part, attributable to its ability to stimulate Nrf2-ARE activation, thereby upregulating a suite of downstream protective genes and proteins, including sod, gsh, catalase, and gpx genes, which collectively contribute to its nephroprotective effects.

The observed modulation of Nrf2, Keap1, HO-1, and KIM-1 gene expression by Q3R aligns with our *in silico* studies, which demonstrated that Q3R exhibits a strong binding affinity and inhibitory activity towards Keap1. By specifically inhibiting Keap1, Q3R releases Nrf2 from its suppressive constraints, allowing the transcription factor to translocate to the nucleus and initiate the expression of a range of antioxidant and cytoprotective genes. [46]

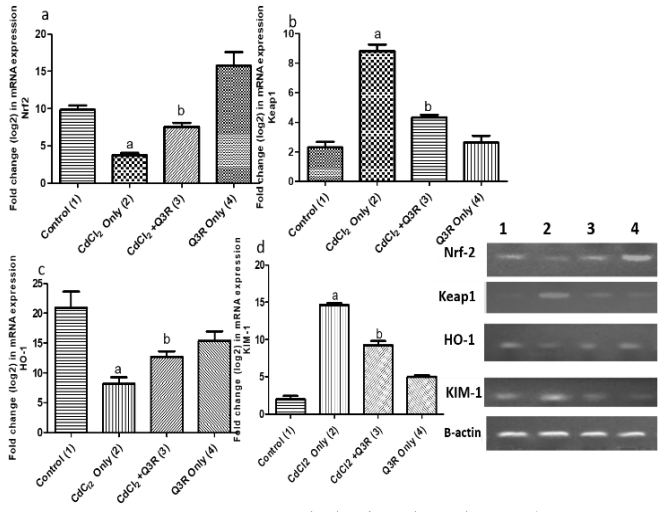

Figure 7: Modulatory effects of Cd and quercetin-3-rhamnoside (Q3R) on the expression of (a) Nrf2, (b) Keap1, (c) HO-1, and (d) KIM-1. Data are presented as mean ± SEM, with distinct superscripts indicating statistically significant differences.

Conclusion

This study highlights the transformative potential of integrating computational (*in silico*) modeling with *in vivo* experimental approaches to advance drug discovery. Our findings robustly demonstrate the renoprotective properties of Q3R in mitigating cadmium-induced kidney injury in mice, supported by results from both predictive simulations and biological assays. To translate these insights into clinical impact, subsequent research should prioritize preclinical trials that assess Q3R's long-term safety, pharmacokinetics, and dose-response dynamics.

Conflict of Interest

The authors declare no conflict of interest.

Author's Declaration

The authors hereby declare that the work presented in this article is original. Any liability for claims relating to this article will be borne by us.

Funding Declaration

This study received financial backing from Nigeria's Tertiary Education Trust Fund (TETFUND) through its 2024 Institution-Based Research (IBR) initiative, awarded to Edo University Iyamho in Edo State, Nigeria.

References

1. Singh A, Sharma A, Verma RK, Chopade RL, Pandit P, Nagar V. Heavy metal contamination of water and their toxic effect on living organisms. IntechOpen. 2022. https://doi.org/10.5772/intechopen.105075.
2. Genchi G, Sinicropi MS, Lauria G, Carocci A, Catalano A. The effects of cadmium toxicity. Int J Environ Res Public Health. 2020; 17(11):3782. https://doi.org/10.3390/ijerph17113782.
3. Kowalczyk P, Sulejczak D, Kleczkowska P, Bukowska-Ośko I, Kucia M, Popiel M, Kaczyńska K. Mitochondrial oxidative stress: A causative factor and therapeutic target in many diseases. Int J Mol Sci. 2021; 22(24):13384. https://doi.org/10.3390/ijms222413384.
4. Chen PY, Qin L, Simons M. TGFβ signaling pathways in human health and disease. Front Mol Biosci. 2023; 10. https://doi.org/10.3389/fmolb.2023.1113061.
5. Gui T, Sun Y, Shimokado A, Muragaki Y. The roles of mitogen-activated protein kinase pathways in TGF-β-induced epithelial-mesenchymal transition. J Signal Transduct. 2012; https://doi.org/10.1155/2012/289243.
6. Falodun A, Igbinosa E. EDITORIAL: Prospects of Microbial Natural Products and Their Biological Entities in Drug Discovery: http://www.doi.org/10.26538/tjpps/v1i1.1. Trop J Phyto and Pharm Sci. 2022; 1(1): 1. Retrieved from https://tjpps.org/index.php/home/article/view/7
7. Iserhienrhien LO, Okolie PN. Phytochemical screening and *in vitro* antioxidant properties of methanol and aqueous leaf extracts of *Geophila obvallata*. AJRB. 2018; 3(2):1-11. https://doi.org/10.9734/AJRB/2018/4505.
8. Iserhienrhien LO, Okolie PN. Protective effect of Geophila obvallata (Shumach) Didr leaf extract and its fractions against cadmium-induced nephrotoxicity in male Wistar rats. Toxicol Rep. 2022; 87-93. https://doi.org/10.1016/j.toxrep.2021.12.008.
9. Iserhienrhien LO, Okolie PN. Acute and subacute toxicity profile of Geophila obvallata (Shumach.) Didr methanol leaf extract on renal and hepatic indices in Wistar rats. Cogent Food Agric. 2020; 6(1):7-14.
10. Iserhienrhien LO, Iyoha A, Memudu A. Renoprotective effect of hyperin against CdCl2 prompted renal damage by activation of Nrf-2/Keap-1 ARE pathway in male mice. Toxicol Mech Methods. 2024. https://doi.org/10.1080/15376516.2024.2329655.
11. Gan F, Lou J, Duan H, Qin Q, Teng Z, Zhou X, Zhou X. Advances in oral drug delivery systems: Challenges and opportunities. Pharm. 2023; 15(2):484. https://doi.org/10.3390/pharmaceutics15020484.
12. Challapa-Mamani MR, Tomás-Alvarado E, Espinoza-Baigorria A, León-Figueroa DA, Sah R, Rodriguez-Morales AJ, Barboza JJ. Molecular docking and molecular dynamics simulations in related to Leishmania donovani: An update and literature review. Trop Med Infect Dis. 2023; 8(10):457. https://doi.org/10.3390/tropicalmed8100457.
13. Bodun DS, Omoboyowa DA, Omotuyi OI, Olugbogi EA, Balogun TA, Ezeh CJ. QSAR-based virtual screening of traditional Chinese medicine for the identification of mitotic kinesin Eg5 inhibitors. Comput Biol Chem. 2023; 104:107865. https://doi.org/10.1016/j.compbiolchem.2023.107865.
14. Schrödinger L. Release 2017–1: Lig Prep. Schrödinger, LLC. 2017.
15. Iserhienrhien LO, Enoyoze GE. Comparative evaluation of antioxidant activity in extracts and fractions from leaves and stem of *Geophila obvallata* (Schumach)Didr. Adv Clin Toxicol. 2024; 9(2):001-009. https://doi.org/10.23880/act-16000309.
16. Lipinski CA. Lead- and drug-like compounds: The rule-of-five revolution. Drug Discov Today Technol. 2004; 1(4):337-341. https://doi.org/10.1016/j.ddtec.2004.11.007.
17. Asagba S, Obi F. Effects of oral cadmium exposure on renal glomerular and tubular functions in the rat. J Appl Sci Environ Manag. 2004; 8(1):29–32. https://doi.org/10.4314/jasem.v8i1.17222.
18. Chen C, Narayanapillai S, Zhang W, Sham YY, Xing C. Rapid identification of Keap1-Nrf2 small-molecule inhibitors through structure-based virtual screening and hit-based substructure search. J Med Chem. 2022; 57(3):1121–1126. https://doi.org/10.1021/jm4017174.
19. Aebi HU. Methods of enzymatic analysis. 3rd ed. Academic Press; 1984.
20. Samira B, Menaceur F, Gasmi S, Lidoughi A, Rais T, Gattel H. Oxidative stress assessment and its relationship with the

prevalence of atherogenic risk in patients with type 2 diabetes. J Diabetes Metab Disord. 2021; 20(1):583-590.
21. Hayashi I, Morishita Y, Imai K, Nakamura M, Nakachi K, Hayashi T. High-throughput spectrophotometric assay of reactive oxygen species in serum. Mutat Res Genet Toxicol Environ Mutagen. 2007; 631(1):55-61. https://doi.org/10.1016/j.mrgentox.2007.04.006.
22. Daniele D, Stewart AJ, Pellegrini N. A review of recent studies on malondialdehyde as a toxic molecule and biological marker of oxidative stress. Nutr Metab Cardiovasc Dis. 2005; 15(4):316-328.
23. Hosten AO. BUN and creatinine. In: Walker HK, Hall WD, Hurst JW, editors. Clinical methods: The history, physical, and laboratory examinations. 3rd ed. Butterworths; 1990.
24. Wang Y, Sun Q, Liu J, Jin F, Dai Z. Cadmium-induced mitochondrial dysfunction in kidney injury. Redox Biol. 2020; 33:101540. https://doi.org/10.1016/j.redox.2020.101540.
25. Nordberg GF, Nordberg BA, Friberg LM. Handbook on the toxicology of metals. Academic Press; 2007.
26. Genheden S, Ryde U. The MM/PBSA and MM/GBSA methods to estimate ligand-binding affinities. Expert Opin Drug Discov. 2015; 10(5):449–461. https://doi.org/10.1517/17460441.2015.1032936.
27. Alzain AA, Mukhtar RM, Abdelmoniem N, Shoaib TH, Osman W, Alsulaimany M, Aljohani AKB. Modulation of NRF2/KEAP1-mediated oxidative stress for cancer treatment by natural products using pharmacophore-based screening, molecular docking, and molecular dynamics studies. Mol. 2023; 28(16):6003. https://doi.org/10.3390/molecules28166003.
28. Alves FS, Rodrigues Do Rego JDA, Da Costa ML, Lobato Da Silva LF, Da Costa RA, Cruz JN. Spectroscopic methods and in silico analyses using density functional theory to characterize and identify piperine alkaloid crystals isolated from pepper (Piper nigrum L.). J Biol Struct Dyn. 2020; 38(9):2792-2799. https://doi.org/10.1080/07391102.2020.1747546.
29. Hagar M, Ahmed HA, Aljohani G, Alhaddad OA. Investigation of some antiviral N-heterocycles as COVID-19 drug: Molecular docking and DFT calculations. Int J Mol Sci. 2020; 21(11):3922. https://doi.org/10.3390/ijms21113922.
30. Salo-Ahen OMH, Alanko I, Bhadane R, Bonvin AMJJ, Honorato RV, Hossain S, Juffer AH, Kabedev A, Lahtela-Kakkonen M, Larsen AS. Molecular dynamics simulations in drug discovery and pharmaceutical development. Processes. 2021; 9(1):71. https://doi.org/10.3390/pr9010071.
31. Liu S, Stanley A, Yadav L, Sudhakar A. JAK2/STAT3 signaling pathway mediates cadmium-induced inflammatory response and renal fibrosis. Ecotoxicol Environ Saf. 2023; 262:115280. https://doi.org/10.1016/j.ecoenv.2023.115280.
32. Liu J, Liu J, Klaassen CD. Cadmium toxicity and its mechanisms in animals. Recent Pat Toxicol. 2010; 4(1):1–12. https://doi.org/10.2174/1877652101004010001.
33. Salehi B, Mishra AP, Nigam M, Sener B, Kilic M, Sharifi-Rad M, Fokou PVT, Martins N, Sharifi-Rad J. Resveratrol: A double-edged sword in health benefits. Biomed. 2018; 6(3):91. https://doi.org/10.3390/biomedicines6030091.
34. Zhang DD. Keap1-Nrf2 signaling pathway: An emerging target for the treatment of oxidative stress-related disorders. Antioxid Redox Signal. 2015; 22(1):29–48. https://doi.org/10.1089/ars.2014.6013.
35. Chi F, Cheng C, Zhang M, Su B, Hou Y, Bai G. Resveratrol targeting NRF2 disrupts the binding between KEAP1 and NRF2-DLG motif to ameliorate oxidative stress damage in mice pulmonary infection. J Ethnopharmacol. 2024; 332:118353. https://doi.org/10.1016/j.jep.2024.118353.
36. Patil R, Das S, Stanley A, Yadav L, Sudhakar A, Varma AK. Optimized hydrophobic interactions and hydrogen bonding at the target-ligand interface leads the pathways of drug-designing. PLoS One. 2010; 5(8):e12029. https://doi.org/10.1371/journal.pone.0012029.
37. Cui J, Feng Y, Yang T, Wang X, Tang H. Computer-aided designing peptide inhibitors of human hematopoietic prostaglandin D2 synthase combined molecular docking and molecular dynamics simulation. Mol. 2023; 28(15):5933. https://doi.org/10.3390/molecules28155933.
38. Velichkova M, Hasson T. Keap1 regulates the oxidation-sensitive shuttling of Nrf2 into and out of the nucleus via a Crm1-dependent nuclear export mechanism. Mol and Cell Bio. 2005; 25(11): 4501–4513. doi: 10.1128/MCB.25.11.4501-4513.2005
39. Kołacz K, Wójcik M, Balcerzyk M. Resveratrol targeting NRF2 disrupts the binding between KEAP1 and NRF2-DLG motif to ameliorate oxidative stress damage in mice pulmonary infection. Int J Environ Res Public Health. 2017; 14(12):1501. https://doi.org/10.3390/ijerph14121501.
40. Dinkova-Kostova AT, Talalay P. Direct and indirect antioxidant activities of isothiocyanates: Their potential in prevention and therapy of human diseases. J Nutr. 2010; 140(1):75–81. https://doi.org/10.3945/jn.109.111336.
41. Grunenwald A, Roumenina LT, Frimat M. Heme oxygenase 1: A defensive mediator in kidney diseases. Int J Mol Sci. 2021; 22(4):2009. https://doi.org/10.3390/ijms22042009.
42. Nath KA, Grande JP, Haggard JJ, Croatt AJ, Katusic ZS, Solovey A, Hebbel RP. Oxidative stress and induction of heme oxygenase-1 in the kidney in sickle cell disease. Am J Pathol. 2001; 158(3):893–903. https://doi.org/10.1016/S0002-9440(10)64037-4.
43. Xiong L, Xie J, Song C, Liu J, Zheng J, Liu C. The activation of Nrf2 and its downstream regulated genes mediates the antioxidative activities of Xueshuan Xinmaining Tablet in human umbilical vein endothelial cells. Evid Based Complement Alternat Med. 2015; 2015:187265. https://doi.org/10.1155/2015/187265.
44. Hammad M, Raftari M, Cesário R, Salma R, Godoy P, Emami SN, Haghdoost S. Roles of oxidative stress and Nrf2 signaling in pathogenic and non-pathogenic cells: A possible general mechanism of resistance to therapy. Antioxidants. 2023; 12(7):1371. https://doi.org/10.3390/antiox12071371.
45. Yan X, Allen D. Chemical Reviews. 2019; 119(18):10520–10594. https://doi.org/10.1021/acs.chemrev.8b00728.
46. Lee JM, Surh YJ. Targeting Keap1-Nrf2 system with natural compounds for cancer chemoprevention and treatment. Mutat Res. 2013; 751(1-2):116–126. https://doi.org/10.1016/j.mrfmmm.2013.06.003.